State-selective dissociation dynamics of an oxygen molecular ion studied with single-harmonic pump and infrared-probe pulses

Y. Malakar,[1] F. Wilhelm,[2] D. Trabert,[2] Kanaka Raju P.,[1] X. Li,[1] W. L. Pearson,[1] W. Cao,[1,*] B. Kaderiya,[1] I. Ben-Itzhak,[1] and A. Rudenko[1]

[1]*J. R. Macdonald Laboratory, Department of Physics, Kansas State University, Manhattan, Kansas 66506, USA*

[2]*Institut für Kernphysik, Universität Frankfurt am Main, Frankfurt D-60486, Germany*

(Received 11 May 2018; published 23 July 2018)

Laser-induced dissociation of a photoionized oxygen molecule is studied employing an extreme-ultraviolet-pump–near-infrared-probe (EUV-NIR pump-probe) technique. A combination of a narrow-band 11th harmonic pump centered at 17.3 eV and a moderate-intensity NIR probe restricts the dissociation dynamics to the pair of low-lying cationic states, $a\,^4\Pi_u$ and $f\,^4\Pi_g$. The measured kinetic energies of the O^+ fragments reveal contributions from one-, two-, and three-photon dissociation pathways (1ω, 2ω, and 3ω) involving these two states. While the yields of the two- and three-photon channels initially rise and then decrease as a function of EUV-NIR delay, the yield of the single-photon pathway rises slower but keeps increasing over the whole delay range studied. This behavior reflects the evolving probability density of the ionic nuclear wave packet at the internuclear distances, where it can undergo resonant 3ω and 1ω transitions from the $a\,^4\Pi_u$ to the $f\,^4\Pi_g$ state of $O_2{}^+$.

DOI: 10.1103/PhysRevA.98.013418

I. INTRODUCTION

The development of ultrafast laser technology has enabled time-resolved studies of femtosecond molecular dynamics and provided tools to control them. Many of the suggested control schemes are based on the modification of molecular potential curves by the electric field of an optical or infrared laser pulse [1–6]. This requires the field to be strong enough to be achieved. For these reasons, molecular response to intense, short laser pulses has been the subject of active experimental and theoretical investigations over the last three decades. Since describing the behavior of a molecule irradiated by an intense laser field still represents a major challenge for theory, most of the early investigations focused on accessible model systems such as hydrogen and its isotopologues. Although the exact full-dimensional *ab initio* treatment involving both electrons is still challenging even for such simple targets, a detailed quantitative understanding of molecular dynamics driven by the intense femtosecond optical or near-infrared (NIR) pulses has been achieved (see [7–9] for reviews). Recently, considerable progress has been made to extend this understanding to more complex systems. The first step in this direction is to address larger diatomic molecules like N_2, CO, and O_2 (see, e.g., Refs. [10–19] for some illustrative examples). Since the exact *ab initio* calculations of molecular dynamics in the presence of strong external field are out of reach, theoretical modeling involving a certain level of approximation and benchmarked by the experimental data is needed to achieve this goal.

Experimentally, time-resolved characterization of ultrafast molecular dynamics is typically realized in a pump-probe experiment. Within this approach, a pump pulse initiates a reaction of interest (in other words, launches a molecular wave packet on certain neutral or ionic states, bound or continuum), that is mapped by a synchronized probe pulse arriving after a variable time delay. Depending on the particular states involved, the common probe schemes include absorption or fluorescence measurement, dissociation, ionization, and Coulomb explosion of the molecule. Both the pump and the probe steps are sensitive to the wavelength of the laser pulses used. Numerous pump-probe experiments focusing on ultrafast aspects of molecular dynamics in strong laser fields employ 800-nm pulses of a Ti:sapphire laser for both steps (see, e.g., Refs. [9,12,13,20–26]). This arrangement, while nowadays routinely providing sub-10-fs temporal resolution, has two significant drawbacks. First, since both pulses interact with the molecule in a similar way, disentangling processes that are initiated and observables that are produced by either pulse is often a challenge. Second, more importantly, the typical interaction mechanism for 800 nm is a multiphoton or strong-field ionization or excitation, which makes a pump pulse at this wavelength nonselective, i.e., it essentially populates all states accessible at that intensity. A natural way to address both of these issues is to use pulses of different wavelengths in each step, and restrict the variety of channels initiated (or, in other words, the number of states populated) by the pump pulse. Depending on a particular process of interest, this can be efficiently achieved by employing ultraviolet (UV) or extreme ultraviolet (EUV) radiation for either step. The latter wavelength range is particularly attractive since it enables using single-photon transitions as a pump or a probe, which often significantly simplifies theoretical description of the corresponding step.

Typical sources of EUV radiation employed in ultrafast pump-probe experiments include those based on high-order harmonic generation (HHG) [27,28] and free-electron lasers (FELs) [29]. Both approaches usually deliver broadband light,

*Present address: Huazhong University of Science and Technology, Wuhan, Hubei, China.

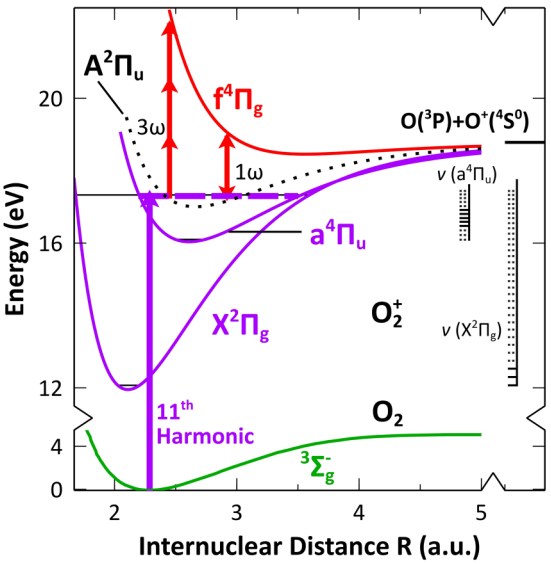

FIG. 1. A sketch of potential energy curves (PECs) for the ground state of O_2 (taken from Ref. [37]) and selected low-lying states of O_2^+ (adapted from Ref. [38]). The purple arrow depicts the EUV-induced photoionization at the equilibrium distance of the neutral molecule, whereas the red arrows indicate the positions of 3ω and 1ω resonant transitions between the $a\,^4\Pi_u$ and $f\,^4\Pi_g$ states [39]. Dashed tick marks on the right indicate the energies of accessible vibrational levels for the $X\,^2\Pi_g$ and $a\,^4\Pi_u$ ionic states. The most abundant vibrational levels in the Franck-Condon region are highlighted with thicker black lines for both states.

as a consequence of the desired ultrashort pulse durations. At the FEL facilities, the lower limit of the bandwidth is usually given by the self-amplified spontaneous emission process used to generate the FEL light. For the HHG sources, many harmonic orders are typically combined to achieve femtosecond or even subfemtosecond pulses. Despite obvious advantages provided by using short pulses, because of their large bandwidth such sources, similar to the NIR pulses, are not well suited for state-selective excitation. Therefore, considerable effort is made to generate rather narrow-band light pulses with both FEL [30–32] and HHG sources [32–36], while still maintaining femtosecond pulse duration, short enough to resolve molecular dynamics of interest.

Here we present the results of a time-resolved study of the interaction of a moderately intense ($\sim 10^{13}$ W/cm^2) NIR laser pulse with a molecular wave packet generated by the photoionization of an oxygen molecule with a narrow-band single-harmonic pulse. We employ a recently developed setup based on a double-grating monochromator briefly described in Ref. [36]. Specifically, we launch an ionic wave packet using an 11th harmonic EUV pulse of ~130 fs duration [full width at half maximum (FWHM) in intensity], with a central photon energy of 17.3 eV and a bandwidth of ~300 meV. Under these conditions, in contrast to earlier experiments employing NIR or broadband EUV pulses, we predominantly populate a small subset of O_2^+ states, namely, the ground state and the metastable $a\,^4\Pi_u$ excited state (see Fig. 1). We probe the dynamics of the created wave packet by dissociating the O_2^+ ion by a 35-fs, 790-nm, $\sim 10^{13}$ W/cm^2 probe pulse, which

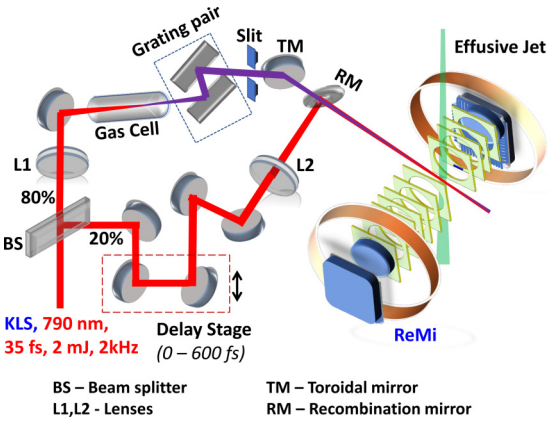

FIG. 2. Sketch of the experimental setup.

at these intensities almost exclusively dissociates the excited state.

By measuring the delay-dependent yields and kinetic energies of the O^+ fragments, we identify three different fragmentation pathways resulting from the net absorption of one, two, or three NIR photons. Our findings are consistent with the dissociation process proceeding via either single- or three-photon coupling to the dissociative $f\,^4\Pi_g$ state, which has been invoked to interpret earlier results obtained with a single, more intense NIR laser pulse [17–19] or using different pump-probe schemes [13,40]. Dominant pathways observed in our experiment closely resemble 1ω and 2ω channels well known for H_2^+ dissociation in the NIR laser field ([41–46]; see also [7,8] for review). For the case of oxygen, we observe a very different dependence on the EUV-NIR delay for these channels, reflecting different times after photoionization at which the ionic nuclear wave packet propagating in the bound $a\,^4\Pi_u$ state of O_2^+ reaches internuclear distances corresponding to resonant one- and three-photon transitions to the $f\,^4\Pi_g$ state. Our results complement a recent experimental study of similar dynamics in an O_2^+ molecular ion triggered by ultrashort but broadband harmonic pulses [40].

II. EXPERIMENT

The setup used here is similar to the one described in [36,47] and is sketched in Fig. 2. A 2-mJ, 35-fs, 790-nm NIR pulse from a Ti:sapphire laser system known as the Kansas Light Source (KLS) at 2-kHz repetition rate is split by a beam splitter. Eighty percent of the pulse energy is focused into a semi-infinite gas cell filled with argon for high-order harmonic generation. A grating based monochromator consisting of a pair of identical holographic blazed gratings (3600 lines/mm) followed by an adjustable slit is installed after the harmonic generation cell. The combination of grating pair and slit allows the selection of a single harmonic. The slit width is used to fine-tune the bandwidth of the harmonic pulse. In this experiment, the selected 11th harmonic is then focused onto an effusive atomic or molecular beam in the center of a "reaction microscope" (ReMi) spectrometer by a toroidal mirror (TM). After the TM, the harmonic beam passes through a hole in a recombination mirror that combines it with the NIR beam. The other part of the laser beam is sent through a delay stage

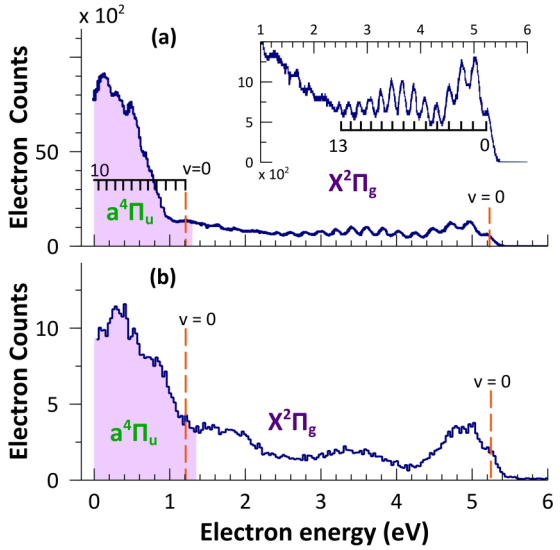

FIG. 3. The measured photoelectron energy distribution for photoionization of O_2 by the 11th harmonic EUV with a bandwidth of $\leqslant$ 200 meV (a) and ~300 meV (b). The inset in (a) shows the enlarged view of the region corresponding to the $X\,^2\Pi_g$ ground state. For this state, contributions from individual vibrational levels are clearly resolved with the narrow-bandwidth EUV pulse. The positions of the individual vibrational levels shown as tick marks are taken from Refs. [48,49] for $X\,^2\Pi_g$ and $a\,^4\Pi_u$ states, respectively.

used to adjust the path and is independently focused onto the same target by a 1-m-focal-length lens. The peak intensity of the NIR probe is set to $\sim 10^{13}$ W/cm^2 such that it alone does not yield any observable dissociative ionization signal from O_2. Ions and electrons created by the interaction of the two light pulses with the target are guided in opposite directions onto two time- and position-sensitive delay-line detectors by electric and magnetic fields applied along the spectrometer axis. During the pump-probe measurement, focused mainly on ion detection, we applied an electric field of 1.26 V/cm. In contrast, to obtain high-resolution electron spectra, field-free conditions were employed. From the measured time of flight and positions of the hits on the detector the full momentum vectors of each detected charged particle are calculated.

The central wavelength and the bandwidth of the 11th harmonic pulse were determined using the photoelectron spectrum resulting from the photoionization of argon atoms. The central wavelength of the 11th harmonic selected for this pump-probe study was 17.3 eV. Even though the smallest bandwidth achievable with our setup can be well below 200 meV [47], for the time-resolved experiment described here it was set to ~300 meV by adjusting the slit width in the monochromator in order to increase the EUV photon flux. The corresponding bandwidth difference can be clearly seen in the O_2 photoelectron spectra for both configurations presented in Fig. 3. While the overall shape of both distributions is pretty similar, the individual vibrational levels of the resulting O_2^+ ion can be clearly resolved only if the 11th harmonic is optimized for a smallest bandwidth [<200 meV, Fig. 3(a)]. For a somewhat larger EUV bandwidth, which we later employed in our pump-probe measurement, the vibrational structure is washed out [Fig. 3(b)].

The corresponding 11th harmonic pulse duration was estimated to be ~130 fs based on the EUV-NIR cross-correlation signal measured using the delay-dependent sidebands in the photoelectron spectrum resulting from the NIR-assisted photoionization of argon. The delay at which this cross-correlation signal reaches its maximum was set as a zero delay for our pump-probe measurement.

III. RESULTS AND DISCUSSION

A. EUV-only photoelectron spectra: Identification of relevant ionic states

As illustrated in Fig. 1, ionization of a neutral O_2 molecule via absorption of an 11th harmonic photon (17.3 eV) predominantly results in the population of one of the two lowest electronic states of the O_2^+ cation: The $X\,^2\Pi_g$ ground state or the $a\,^4\Pi_u$ excited state, usually associated with the removal of an electron from the π_g highest occupied molecular orbital (HOMO) or the $3\sigma_g$ HOMO-1, respectively. The population of both states is reflected in the kinetic energy distribution of emitted photoelectrons as shown in Fig. 3. The spectrum displayed in Fig. 3(a), which was obtained with the EUV pulse of sub-200-meV bandwidth, shows that a broad distribution of vibrational states (resolved up to $\nu = 13$) is populated in the ground electronic state of the ion. The results shown in Fig. 3(b), for a somewhat broader bandwidth, resemble the data of Fig. 3(a), but individual vibrational states are not resolved. For the $a\,^4\Pi_u$ state, the highest vibrational level energetically accessible by the 17.3-eV photon is $\nu = 10$ [considering the bandwidth, states with $\nu = 11$ and $\nu = 11,12$ can also be populated for the conditions of Fig. 3(a) and 3(b), respectively]. Even though single vibrational levels are not clearly resolved for the $a\,^4\Pi_u$ state even for narrow-bandwidth pulses (most likely because of the smaller vibrational spacing), the observed low-energy peak in the photoelectron spectrum of Fig. 3 indicates that a significant fraction of O_2^+ ions end up in this state. It should be noted that because of the limited photoelectron collection efficiency under field-free conditions employed to obtain the spectra shown in Fig. 3, the energy distribution presented here does not directly reflect the branching ratio of the populations of the corresponding electronic and vibrational states.

As sketched in Fig. 1, the vibrational levels of the $a\,^4\Pi_u$ state accessible under our experimental conditions overlap in energy with high-lying ($\nu = 21$ to $\nu = 31$) vibrational levels of the $X\,^2\Pi_g$ ground cationic state. However, according to the Franck-Condon factors for the photoionization of O_2 [50,51], the populations of these high vibrational levels of the $X\,^2\Pi_g$ state are expected to be considerably smaller than for the low (up to $\nu = 12$) vibrational levels of the $a\,^4\Pi_u$ state.

In addition to the contributions from the two dominant electronic states discussed above, some ionization events at our photon energy might in principle populate the lowest vibrational levels of the $A\,^2\Pi_u$ state of O_2^+, as indicated in Fig. 1. The corresponding contribution in the photoelectron spectra would be indistinguishable from that of higher vibrational states of $a\,^4\Pi_u$. However, from earlier experiments employing threshold photoelectron spectroscopy [44,45] or fluorescence measurements [52], as well as from the calculation of the

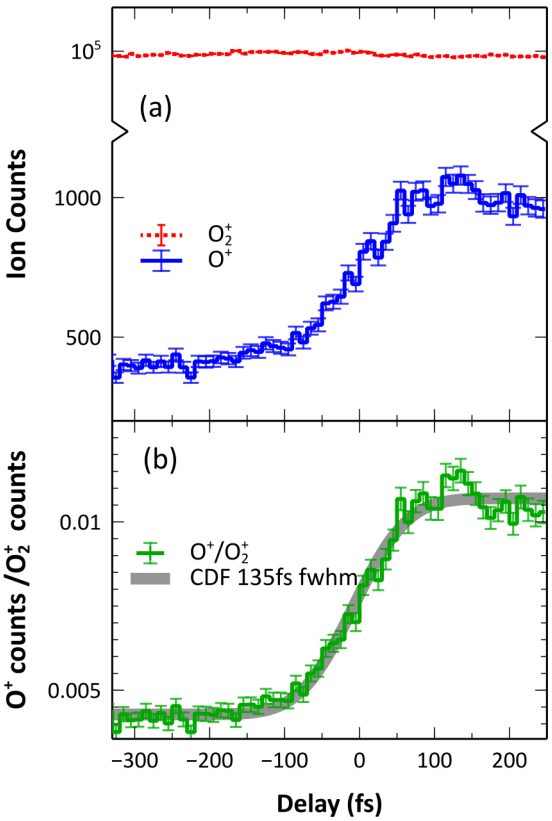

FIG. 4. (a) The measured yields of $O_2{}^+$ (dotted red line) and O^+ (solid blue line) ions as a function of EUV-NIR delay. (b) The measured ratio of $O^+/O_2{}^+$ yields as a function of EUV-NIR delay. The shaded gray line depicts the Gaussian cumulative distribution function (CDF) corresponding to the overlap between the EUV and NIR pulses defined form their measured cross correlation (see text).

corresponding partial ionization cross sections [53] we can conclude that the population of the $A\,^2\Pi_u$ state at 17.3 eV is negligibly small compared to that of the $a\,^4\Pi_u$ state.

B. Dissociation pathways and kinetic energy release spectra

Since our EUV photon energy lies well below the lowest dissociative ionization limit (18.733 eV [49]), the 11th harmonic alone does not create any O^+ fragments. However, if the NIR pulse is combined with the 11th harmonic, the molecular ion can dissociate. Figure 4(a) depicts the yields of $O_2{}^+$ (dotted red line) and O^+ (solid blue line) ions measured in a two-color 11th harmonic pump–NIR-probe experiment as a function of EUV-NIR delay. The $O_2{}^+$ signal contains ions produced by either single-photon EUV or multiphoton NIR ionization, and does not show any pronounced delay dependence. The deviation of the delay-dependent $O_2{}^+$ yield from the flat line mainly reflects the instability of the flux of generated harmonics. On the contrary, the O^+ yield increases significantly at positive delays, where the NIR pulse arrives after the EUV. In order to account for long-term laser instabilities, we plot the delay-dependent ratio of the O^+ and the $O_2{}^+$ ion yields in Fig. 4(b). The O^+ signal at large negative delays essentially represents the delay-independent background, mainly originating from two sources. The first one is the dissociative ionization of water from the residual gas. The other, and more important one, originates from O_2 dissociative ionization by the harmonics orders higher than the 11th, mainly from the second diffraction order of the 21st and 23rd harmonics as they also pass through the slit (see Ref. [47] for details). In a region of ± 100 fs around zero delay the measured yield rises, reflecting the increased production of O^+ fragments due to the combined action of the EUV and the NIR pulses. It exhibits a broad maximum between 100 and 150 fs, and then slightly decreases.

Qualitatively, the enhanced O^+ fragments production at positive delays can be readily understood as NIR-induced dissociation of the $O_2{}^+$ cations produced by the ionization of the neutral O_2 molecule by 11th harmonic photons. The timescale for the rise of the O^+ yield, which starts well before zero delay, essentially reflects a rather broad region where the NIR and EUV pulses overlap. In order to visualize the influence of the combined pulse widths on the delay-dependent O^+ signal, we plot in Fig. 4(b) the Gaussian cumulative distribution function (CDF) given by

$$Y(t) = \frac{h}{2}\left[1 + \mathrm{erf}\left(\frac{t-\mu}{\sqrt{2\sigma^2}}\right)\right] + l. \qquad (1)$$

Here, h and l are the asymptotic high and low limits of the signal, respectively; $\mu = 0$ is the center position and $\sigma = 57$ fs is the Gaussian width of the experimentally determined EUV-NIR cross correlation (135 $\pm$ 20 fs FWHM). The CDF with the above parameters, which essentially reflects a convolution of a step-function yield with the temporal resolution of the experiment, matches well the rising part of the measured curve shown in Fig. 4(b).

In order to understand in detail the mechanisms of two-color dissociative ionization leading to the nonmonotonic delay-dependent signal shown in Fig. 4, we analyze the kinetic energies of the O^+ fragments. Figure 5(a) displays the measured kinetic energy release (KER) distribution of $O^+ + O$ pairs integrated over all EUV-NIR delays. Note that since the sum momentum of all absorbed photons and the emitted electron is much smaller than the momenta of the nuclei, for each dissociative ionization event the neutral and ionic oxygen fragments carry the same energy due to momentum conservation. Therefore, the KER values shown in Fig. 5 are calculated from the measured O^+ kinetic energies simply by multiplying by 2.

The KER spectrum peaks at zero energy and exhibits a broader structure between 0.6 and 3 eV. The lowest dissociation limit of $O_2{}^+$ (18.733 eV) is energetically accessible by a single 790-nm photon transition from the $a\,^4\Pi_u$ state starting from the $v = 10$ vibrational level [19]. Even though the $v = 9$ state lies below the dissociation threshold for our central NIR wavelength, given the 65-nm bandwidth of the NIR pulse, it might dissociate contributing to the region of the lowest KER. The KER values corresponding to the absorption of two NIR photons from different vibrational levels of the $a\,^4\Pi_u$ state match the broad structure centered at $\sim$1.5 eV, whereas the events with the KER beyond 1.9 eV need at least three-photon absorption from the same electronic state. There, the measured fragment yield decreases fast with the increasing energy. As indicated in Fig. 5, we refer to these regions as 1ω, 2ω, and 3ω respectively.

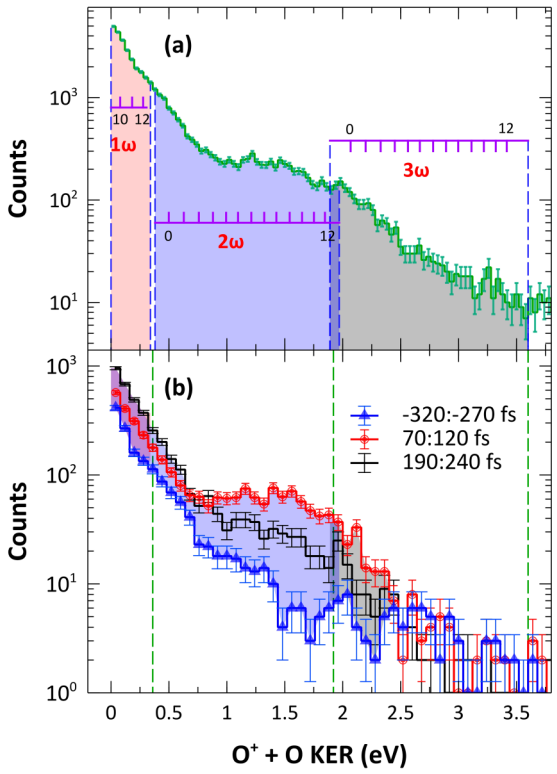

FIG. 5. (a) Kinetic energy release (KER) distribution of the O + O^+ channel integrated over all EUV-IR delays. Vertical dashed lines indicate the KER values expected for $O_2{}^+$ dissociation via 1ω, 2ω, and 3ω transitions from different vibrational levels of the $a\,^4\Pi_u$ to the $f\,^4\Pi_g$ state at 790 nm. Shadowed areas depict the range of KER expected for each transition considering the bandwidth of the NIR-probe pulse. (b) KER distributions for three different EUV-NIR delay regions.

Dissociation of the $O_2{}^+$ molecules that are left in the $X\,^2\Pi_g$ ground state after the EUV pulse requires absorption of one NIR photon for levels $v > 28$, at least two NIR photons for levels with $v > 17$, at least three photons for $v > 9$, and at least four photons for lower vibrational states. However, as indicated in Fig. 1, the Franck-Condon factors for O_2 strongly favor the population of the lower vibrational states [50,51]. Correspondingly, at the rather low NIR intensity used in our experiment one would expect the transitions from the $a\,^4\Pi_u$ state involving fewer NIR photons to dominate the dissociation process, even though we could not exclude some contributions from the cationic ground state, especially in the low-energy region. It should be noted that in earlier experiments [13,17–19], no clear signatures of the $X\,^2\Pi_g$ state contributions to the dissociation dynamics have been reported even for much higher NIR intensities (up to 10^{15} W/cm^2).

The KER spectrum presented in Fig. 5(a) can be understood under the assumption that the dominant contribution to the NIR dissociation of $O_2{}^+$ originates from the transition between the $a\,^4\Pi_u$ state and the $f\,^4\Pi_g$ state. Indeed, as can be seen in Fig. 1, one NIR photon can directly couple these two curves, resulting in the 1ω channel. The dipole selection rules forbid the direct two-photon transition between the $a\,^4\Pi_u$ and $f\,^4\Pi_g$ states. Therefore, as discussed in Refs. [13,17–19,54–56], the 2ω pathway most likely occurs via one of the two following pathways. The first one proceeds via the resonant absorption of three NIR photons from the $a\,^4\Pi_u$ to the $f\,^4\Pi_g$ state, and subsequent stimulated emission of one NIR photon as the wave packet passes through the position of the resonant 1ω transition between the two states as shown in Fig. 1. An alternative possible two-photon pathway, which will be discussed in Sec. III D, involves a one-photon transition from the $a\,^4\Pi_u$ to the $f\,^4\Pi_g$ state, and subsequent one-photon transition from the $f\,^4\Pi_g$ to the $^4\Sigma_u^+$ state [18].

Similar one-photon and (net) two-photon (1ω and 2ω) dissociation pathways are well documented for H_2 and D_2 fragmentation in intense NIR fields [7,8,41–46]. In Fig. 5 we also clearly observe a high-energy tail formed by the 3ω channel, i.e., by the events which were triggered by a three-photon transition and did not undergo stimulated emission at a larger internuclear distance corresponding to one-photon resonance. In many experiments with a H_2/D_2 target at 800 nm this channel is hidden beneath the low-energy tail of the Coulomb explosion pathway. However, it was clearly observed in earlier measurements on H_2 dissociation with a 532-nm laser [57], and in the experiment employing a $H_2{}^+$ ion beam target and few-cycle 800-nm pulses [58,59]. Since in the present study we do not observe any Coulomb explosion events due to the selected NIR intensity, the tail of our high KER spectrum is in accord with the expectation for the 3ω channel.

C. Delay-dependent dynamics

As can be seen from Fig. 1, the 3ω transition between the $a\,^4\Pi_u$ and $f\,^4\Pi_g$ states occurs close to the Franck-Condon region, whereas the single-photon transition between these two states requires a considerably larger internuclear distance. This should be reflected in the time evolution of the corresponding dissociation channels. From Fig. 5(b), where the KER distributions for three different EUV-NIR delay regions are shown, it is clear that the branching ratio of different dissociation channels changes with the delay. In particular, the spectrum in the range of 70–120 fs contains a significantly higher fraction of high-energy fragments (2ω and 3ω channels) compared to large positive or negative delays. In order to investigate this in more detail, we plot in Fig. 6 the KER of all $O^+ + O$ dissociation channels as a function of the delay between the 11th harmonic EUV pump and NIR-probe pulses. Since our EUV pulse duration is considerably longer than the $O_2{}^+$ vibrational period, we do not resolve signatures of the vibrational motion here. Nevertheless, different KER regions exhibit different delay dependence, as can be clearly seen from Fig. 6. Specifically, while the yield of low-energy fragments reaches its maximum at the largest EUV-NIR delays, the yield of high-energy fragments peaks just before 100 fs and then decreases.

In order to quantify this difference, we plot the delay-dependent yields of 3ω (a), 2ω (b), and 1ω (c) channels in Fig. 7. Similar to the data of Fig. 4(b), all three curves are divided by the delay-dependent $O_2{}^+$ yield. To obtain a clean delay dependence, while selecting the data for the three curves shown in Fig. 7, we excluded the energy regions where different channels overlap. All three channels in Figs. 7(a)–7(c) manifest a pronounced rise in the region of the time overlap between the EUV pump and NIR-probe pulses. To estimate

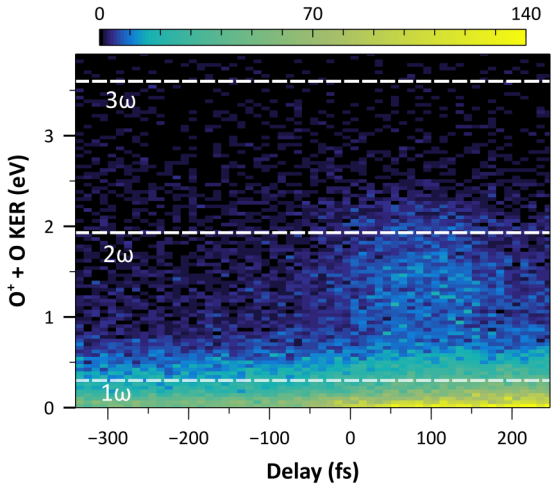

FIG. 6. The measured KER distribution for $O + O^+$ dissociation fragments as a function of EUV-IR delay. The dashed lines separate the contributions from different channels corresponding to the KER regions indicated in Fig. 5.

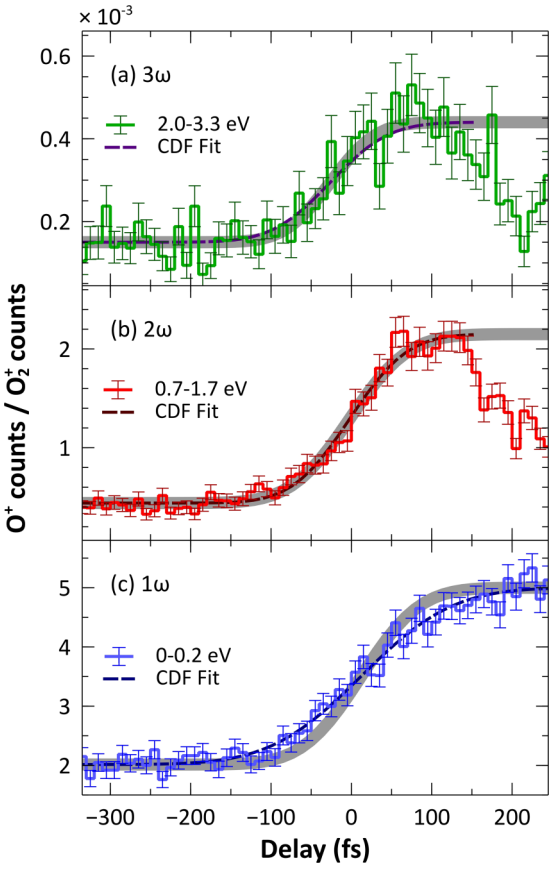

FIG. 7. Delay-dependent ratio of O^+ to O_2^+ yields for three different KER regions associated with 3ω, 2ω, and 1ω transitions, respectively: (a) 2–3.3 eV; (b) 0.7–1.7 eV; (c) 0–0.2 eV. Dashed lines represent the Gaussian CDF fits to the data. Shaded gray line in all panels depicts the CDF with the Gaussian width of $\sigma = 57$ fs corresponding to the measured cross correlation of the EUV and NIR pulses [identical to the CDF shown in Fig. 4(b)].

the timescale of this rise, we fit all three distributions with the Gaussian CDF. While the rising yields of the 3ω and 2ω channels [Figs. 7(a) and 7(b)] exhibit time constants similar to each other and to the cross-correlation of the EUV and NIR pulses within the precision of our experiment (Gaussian width of the CDF fit $\sigma = 46 \pm 12$ fs and $\sigma = 57 \pm 5$ fs for 3ω and 2ω, respectively), the 1ω signal rises considerably slower ($\sigma = 89 \pm 7$ fs). Furthermore, there is a pronounced qualitative difference: While the yield of the 1ω channel increases continuously, becoming flat at the largest delays studied, the yields of the other two channels drop down after reaching their maximum around 100 fs. This behavior can be qualitatively understood by considering the internuclear distances for three-photon and one-photon transitions between the $a\,^4\Pi_u$ and $f\,^4\Pi_g$ states, as discussed below.

After the vertical transition corresponding to the EUV ionization of the neutral molecule, part of the molecular wave packet contributing to the NIR dissociation propagates outwards on the $a\,^4\Pi_u$ potential well. As discussed above, both 3ω and 2ω channels likely result from the three-photon excitation, which occurs rather close to the Franck-Condon region (see Fig. 1). Correspondingly, this NIR-driven transition can occur right after the EUV photoabsorption, and, thus, the yields of the resulting dissociation channels rise on the same timescale as the Gaussian CDF with the parameters defined from the measured cross correlation between the EUV and the NIR pulses (shaded gray lines in Fig. 7). In contrast, the one-photon transition between the two states involved can happen only at larger internuclear distances and, thus, at later times after the EUV absorption. This results in the slower rise of the 1ω channel. The time the wave packet needs to travel on the $a\,^4\Pi_u$ state between the positions where the three-photon and one-photon transitions are resonant is estimated to be of order of 10 fs. While the observed rise times of the delay-dependent yields of the 3ω and 2ω channels are similar to each other, the rise time of the yield of the 1ω channel is noticeably longer. The observed difference is considerably larger than 10 fs, and is comparable to the full vibrational cycle (~35 fs for the lowest vibrational levels of the $a\,^4\Pi_u$ state or ~40–45 fs for the vibrational states accessible with one NIR photon). Even though the temporal resolution of the present experiment does not allow us to determine the origin of this difference unambiguously, we consider two potential reasons for this behavior. First, since the repulsive $f\,^4\Pi_g$ curve is considerably flatter in the vicinity of the 1ω resonance, the nuclear wave packet can undergo a one-photon transition over a broader range of internuclear distances than a three-photon transition. This makes the time when the wave packet passes the region of the 1ω coupling less well defined, broadening the rise time of the 1ω channel. Second, a single-photon transition responsible for the 1ω channel does not require the highest laser intensity within the NIR-probe pulse, which makes the effective NIR laser pulse duration longer than its FWHM, potentially contributing to the slower rise time of this channel.

After the initial EUV absorption, a portion of the vibrating nuclear wave packet will return to the position of the three-photon resonance after each vibrational cycle. Nevertheless, since the three-photon transition lies in the inner, steeper part of the $a\,^4\Pi_u$ potential well, the probability to find the wave packet in a rather narrow window accessible for this transition

in the later cycles will be smaller than its initial value right after the EUV absorption. This behavior has been shown in the nuclear wave packet simulations for other diatomics, where, similar to our case, the wave-packet propagation started close to the inner turning point of the asymmetric potential well [60–62]. Correspondingly, the yields of both channels resulting from the three-photon transition decrease with the increasing delays between the EUV and NIR pulses beyond their temporal overlap region. As was shown in Refs. [61,62], the probability density for the portion of the wave packet reaching the inner turning point flattens after a couple of vibrational cycles. This is consistent with the observed fall-off time of our 2ω and 3ω signals. Correspondingly, the delay-dependent yield of the 1ω channel flattens on a similar timescale after the EUV-NIR temporal overlap region. In order to achieve more quantitative understanding of the observed delay dependence of different dissociation channels, a detailed wavepacket propagation simulation taking into account R-dependent transition probabilities between the $a\,^4\Pi_u$ and $f\,^4\Pi_g$ states is needed.

D. Comparison with previous work

The results we present here complement a variety of earlier experiments studying the $O_2{}^+$ dissociation by intense NIR laser fields (e.g., [13,17–19,40]). Those can be separated into single-pulse experiments starting with either a neutral O_2 target [17,19] or with an $O_2{}^+$ ion beam [18,19], and pump-probe experiments employing either two NIR pulses [13] or EUV-pump–NIR-probe configuration [40]. The most straightforward comparison can be made with the latter experiment [40]. The main difference between the two experiments is that Cörlin *et al.* [40] used a much broader spectrum of the EUV pump pulse (harmonic train), but had considerably shorter temporal duration as compared to the present one. Correspondingly, the vibrational motion of the created ionic wave packet could be resolved in time, but many states were directly populated by the pump pulse, including several dissociating states. In order to simplify the analysis of the time-dependent data, the NIR-probe pulse intensity in [40] was chosen rather low (5×10^{12} W/cm^2), such that only one-photon NIR transitions could play a role. Therefore, Cörlin *et al.* concluded that the observed dissociation dynamics for the low-energy region can be fully accounted for by considering a single-photon transition from the $a\,^4\Pi_u$ to $f\,^4\Pi_g$ state induced by the probe, which is consistent with our observations. In Ref. [40] no data for higher O^+ energies corresponding to our 2ω and 3ω channels were presented, most likely because this region is dominated by the direct single-photon dissociation induced by the broadband EUV pump.

For the pump-probe experiment with two sub-10 fs NIR pulses [13], the measured KER-resolved Fourier spectra were interpreted in terms of one- and two-photon transitions from the $a\,^4\Pi_u$ to $f\,^4\Pi_g$ states, and no clear contributions from the ground ionic state had been observed even though the probe intensity was more than an order of magnitude higher than in the present experiment. The authors of Ref. [13] pointed out a certain discrepancy between their measured frequencies of the wave-packet vibrational motion and the expected frequencies for the corresponding vibrational levels of the $a\,^4\Pi_u$ state. In a recent theoretical analysis [56] this discrepancy was attributed to the contribution from the higher-lying $b\,^4\Sigma_g^-$ state of $O_2{}^+$. Since this state is not accessible by our 17.3 eV pump photon, this state is unlikely to contribute significantly to the dissociation signal observed in our work.

It is interesting to compare our observations with the results obtained in a single-pulse experiments starting with ionic targets [18,19]. Since the ionic target for these experiments is produced predominantly in the $X\,^2\Pi_g$ ground and $a\,^4\Pi_u$ excited electronic states, this arrangement to a large extent resembles the conditions for the probe step of our experiment. In the KER spectra obtained in Ref. [18] contributions from all three dissociation channels discussed in this work were identified. In addition, a few other dissociation pathways starting from the $a\,^4\Pi_u$ state and involving one-photon coupling to the $f\,^4\Pi_g$ state followed by sequential one- or two-photon transitions to some higher-lying states were found to contribute to the KER spectra at the high-energy part of our 2ω channel. These contributions were identified by their specific angular distributions, considered in combination with the measured KER values and the corresponding selection rules. In particular, the dominant contribution to the 2ω channel was found to come from the pathway involving a one-photon transition from the $a\,^4\Pi_u$ to the $f\,^4\Pi_g$ state, and subsequent one-photon transition from the $f\,^4\Pi_g$ to the $^4\Sigma_u^+$ state. This assignment was based on a characteristic four-lobe angular distribution resulting from a combination of the parallel and the perpendicular transitions [18].

Even though we cannot derive a definite conclusion from the angular distributions of the fragment ions, a very similar delay dependence we observe for the 2ω and 3ω channels suggests that in our measurement the dissociation proceeding via net two- and three-photon absorption predominantly occurs via a three-photon resonant transition from the $a\,^4\Pi_u$ to the $f\,^4\Pi_g$ state. Following this transition, a certain fraction of the wave packet just dissociates along the $f\,^4\Pi_g$ curve (3ω), and another part ends up on the $a\,^4\Pi_u$ curve via stimulated emission of one photon at larger internuclear distances, energetically corresponding to the net two-photon absorption (2ω). The absence of clear signatures of the alternative 2ω pathway identified in Ref. [18] in our data is likely due to a different initial vibrational distribution of the $a\,^4\Pi_u$ state population, which is centered at $v = 2$ for the ion beam target used in Ref. [18], and is expected to be shifted towards higher v in our case (see Fig. 1 and Refs. [50,51]). This hypothesis, which implies that the resonant 3ω transition played a lesser role for the results of Refs. [18,19] than for the present experiment, is further supported by the fact that the peak associated with the 3ω transition in Ref. [18] was not observed at all the NIR pulse intensities below 1.6×10^{14} W/cm^2, which is more than an order of magnitude higher than the NIR intensity used in the present experiment. Nevertheless, a certain contribution from the $a\,^4\Pi_u \rightarrow f\,^4\Pi_g \rightarrow {}^4\Sigma_u^+$ pathway can be present in our 2ω channel.

Finally, the interpretation of the results of single-pulse experiments on the NIR-induced dissociation of a neutral O_2 target [17,19] needs to take into account the anisotropy of the molecular ensemble created by the initial ionization step. Nevertheless, the outcome of these experiments also seems to be consistent with our findings. Vibrationally resolved analyses

of the 1ω channel for the neutral O_2 target performed in [19] at the NIR intensity of 10^{14} W/cm^2 indicated that the observed low-energy O^+ fragments are produced via the $a\,^4\Pi_u$ excited state of the $O_2{}^+$ ion rather than the cationic ground state. On the other hand, the angular distributions of the O^+ ions measured in Ref. [17] at the intensity of 2×10^{14} W/cm^2 suggest that the dissociation process proceeds predominantly via parallel transitions for all 1ω, 2ω, and 3ω channels. This indicates that the most likely dissociation pathways in that experiment are driven by the one- or three-photon couplings between the $a\,^4\Pi_u$ and the $f\,^4\Pi_g$ cationic states.

IV. CONCLUSION AND OUTLOOK

In this work, the dynamics of dissociative ionization of an O_2 molecule is investigated in a time-resolved experiment employing 11th harmonic EUV pump and NIR-probe pulses. The selection of single-order, narrow-band 11th harmonic pulse allows preparing the $O_2{}^+$ molecular ion in two specific cationic states, the ground $X\,^2\Pi_g$ and excited $a\,^4\Pi_u$ states, whereas the choice of rather low NIR-probe intensity almost exclusively restricts the dissociation pathways to the ions created in the excited state. Moreover, despite the abundance of dissociating cationic states, which might be accessible by sequential few-photon transitions, under our conditions both, the kinetic energy spectra and the delay dependence of all three dissociation channels observed are consistent with dissociation processes involving only a single low-lying curve, the $f\,^4\Pi_g$ state. This behavior to a large extent mimics the NIR-induced dissociation mechanisms for the $H_2{}^+/D_2{}^+$ molecular ion governed by the dynamics on the $1s\sigma_g$ ground and $2p\sigma_u$ excited states, which have served as the main test grounds for studying laser-molecule interactions and developing theoretical models during last three decades [7,8].

The experimental technique employed here allows one to restrict the number of fragmentation pathways of a multielectron molecule like O_2 to a few states. This can be efficiently exploited for benchmarking molecular dynamics calculations and for visualizing the modification of molecular potential curves in the external light field [6]. Selecting different harmonic orders, one can adapt this experimental arrangement to studies of either highly excited states of neutral molecules, or a variety of ionic states. Two key modifications of the present experimental setup would make it a powerful tool for these applications. The first one is improving the present ion momentum resolution, which is mainly limited by the use of the effusive molecular beam target. The corresponding uncertainty in the initial target momentum is the most likely reason for our inability to resolve the contributions from individual vibrational levels in the KER spectra of $O_2{}^+$ ions shown in Figs. 5 and 6, which were clearly resolved in [13,19].

The second modification is the implementation of three-dimensional (3D) momentum-resolved coincident ion-electron detection. Even though the latter feature can be to some extent realized for the conditions of the present experiment, our current combination of target geometry and imaging system makes it difficult to achieve reasonable resolution for ions and electrons simultaneously (recall that the high-resolution electron spectra presented in Fig. 3 were obtained under field-free conditions). Since the effusive target was used to increase the event rate by increasing the target density, both of the modifications mentioned above can be readily implemented if a few-mJ, multi-10-kHz laser system were used for such experiments. The increased repetition rate would allow replacing the effusive target with a supersonic molecular beam and make coincident measurements more efficient. This, in turn, would enable the so-called kinematically complete experiments on dissociation of molecular cations, where the momentum of the undetected neutral fragment is reconstructed from the measured ion and electron momentum employing momentum conservation [63].

Finally, rather narrow EUV bandwidth ($\sim$300 meV), which enables the state-selective excitation, can be combined with a pulse duration much shorter than the one used in this work. The Fourier-transform limit (FTL) of such EUV pulse is shorter than 10 fs. Even though compression to the FTL value is not feasible, by using a time-delay compensated monochromator with our current bandwidth one could achieve pulse durations shorter than the vibrational period of the relevant molecular states (for the price of reduced EUV photon flux) [32,33]. This would allow combining state selectivity with time resolution better than the vibrational period, thus, enabling KER vs frequency analysis similar to the one presented in [13,22]. Along with the coincident photoelectron detection mentioned above, this would deliver a set of experimental tools for comprehensive characterization of the structure and dynamics of molecular states of interest, either field free, or laser dressed.

ACKNOWLEDGMENTS

The authors thank K.D. Carnes for his support in setting up and operating the data aqcuisition and analysis system, A. Vajdi and V. Kumarappan for operating the KLS laser, and A. T. Le and S. J. Robatjazi for valuable discussions. This work was supported by the Chemical Sciences, Geosciences, and Biosciences Division, Office of Basic Energy Sciences, Office of Science, U.S. Department of Energy under Award No. DE-FG02-86ER13491. K.R.P. and W.L.P. were partly funded by the National Science Foundation EPSCoR Track II Award No. IIA-1430493. F.W. acknowledges support from the German DAAD Rise foundation (Project No. US-PH-708). We also wish to thank Professor R. Dörner for his guidance on the DAAD Rise project.

[1] P. Brumer and M. Shapiro, Laser control of molecular processes, Annu. Rev. Phys. Chem. **43**, 257 (1992).

[2] R. S. Judson and H. Rabitz, Teaching Lasers to Control Molecules, Phys. Rev. Lett. **68**, 1500 (1992).

[3] E. D. Potter, J. L. Herek, S. Pedersen, Q. Liu, and A. H. Zewail, Femtosecond laser control of a chemical reaction, Nature **355**, 66 (1992).

[4] A. Assion, T. Baumert, M. Bergt, T. Brixner, B. Kiefer, V. Seyfried, M. Strehle, and G. Gerber, Control of chemical

reactions by feedback-optimized phase-shaped femtosecond laser pulses, Science **282**, 919 (1998).

[5] E. Wells, C. E. Rallis, M. Zohrabi, R. Siemering, B. Jochim, P. R. Andrews, U. Ablikim, B. Gaire, S. De, K. D. Carnes, B. Bergues, R. de Vivie-Riedle, M. F. Kling, and I. Ben-Itzhak, Adaptive strong-field control of chemical dynamics guided by three-dimensional momentum imaging, Nat. Commun. **4**, 2895 (2013).

[6] M. E. Corrales, J. González-Vázquez, G. Balerdi, I. R. Solá, R. de Nalda, and L. Bañares, Control of ultrafast molecular photodissociation by laser-field-induced potentials, Nat. Chem. **6**, 785 (2014).

[7] A. Giusti-Suzor, F. H. Mies, L. F. Dimauro, E. Charron, and B. Yang, Dynamics of H_2^+ in intense laser fields, J. Phys. B **28**, 309 (1995).

[8] J. H. Posthumus, The dynamics of small molecules in intense laser fields, Rep. Prog. Phys. **67**, 623 (2004).

[9] C. R. Calvert, W. A. Bryan, W. R. Newell, and I. D. Williams, Time-resolved studies of ultrafast wavepacket dynamics in hydrogen molecules, Phys. Rep. **491**, 1 (2010).

[10] K. Codling and L. J. Frasinski, Dissociative ionization of small molecules in intense laser fields, J. Phys. B **26**, 783 (1993).

[11] C. Cornaggia, J. Lavancier, D. Normand, J. Morellec, P. Agostini, J. P. Chambaret, and A. Antonetti, Multielectron dissociative ionization of diatomic molecules in an intense femtosecond laser field, Phys. Rev. A **44**, 4499 (1991).

[12] I. A. Bocharova, A. S. Alnaser, U. Thumm, T. Niederhausen, D. Ray, C. L. Cocke, and I. V. Litvinyuk, Time-resolved Coulomb-explosion imaging of nuclear wave-packet dynamics induced in diatomic molecules by intense few-cycle laser pulses, Phys. Rev. A **83**, 013417 (2011).

[13] S. De, M. Magrakvelidze, I. A. Bocharova, D. Ray, W. Cao, I. Znakovskaya, H. Li, Z. Wang, G. Laurent, U. Thumm, M. F. Kling, I. V. Litvinyuk, I. Ben-Itzhak, and C. L. Cocke, Following dynamic nuclear wave packets in N_2, O_2, and CO with few-cycle infrared pulses, Phys. Rev. A **84**, 043410 (2011).

[14] B. L. J. Bakker and D. H. Parker, Photophysics of O_2 excited by tunable laser radiation around 193 nm, J. Chem. Phys. **112**, 4037 (2000).

[15] B. L. J. Bakker, D. H. Parker, P. C. Samartzis, and T. N. Kitsopoulos, Nonresonant photofragmentation/ionization dynamics of O_2 using picosecond and femtosecond laser pulses at 248 nm, J. Chem. Phys. **112**, 5654 (2000).

[16] C. Guo, M. Li, J. P. Nibarger, and G. N. Gibson, Single and double ionization of diatomic molecules in strong laser fields, Phys. Rev. A **58**, R4271 (1998); Nonsequential double ionization of molecular fragments, **61**, 033413 (2000).

[17] A. Hishikawa, S. Liu, A. Iwasaki, and K. Yamanouchi, Light-induced multiple electronic-state coupling of O_2^+ in intense laser fields, J. Chem. Phys. **114**, 9856 (2001).

[18] A. M. Sayler, P. Q. Wang, K. D. Carnes, B. D. Esry, and I. Ben-Itzhak, Determining laser-induced dissociation pathways of multielectron diatomic molecules: Application to the dissociation of O_2^+ by high-intensity ultrashort pulses, Phys. Rev. A **75**, 063420 (2007).

[19] M. Zohrabi, J. McKenna, B. Gaire, N. G. Johnson, K. D. Carnes, S. De, I. A. Bocharova, M. Magrakvelidze, D. Ray, I. V. Litvinyuk, C. L. Cocke, and I. Ben-Itzhak, Vibrationally resolved structure in O_2^+ dissociation induced by intense ultrashort laser pulses, Phys. Rev. A **83**, 053405 (2011).

[20] A. S. Alnaser, B. Ulrich, X. M. Tong, I. V. Litvinyuk, C. M. Maharjan, P. Ranitovic, T. Osipov, R. Ali, S. Ghimire, Z. Chang, C. D. Lin, and C. L. Cocke, Simultaneous real-time tracking of wave packets evolving on two different potential curves in H_2^+ and D_2^+, Phys. Rev. A **72**, 030702(R) (2005).

[21] Th. Ergler, A. Rudenko, B. Feuerstein, K. Zrost, C. D. Schröter, R. Moshammer, and J. Ullrich, Spatiotemporal Imaging of Ultrafast Molecular Motion: Collapse and Revival of the D_2^+ Nuclear Wave Packet, Phys. Rev. Lett. **97**, 193001 (2006).

[22] B. Feuerstein, Th. Ergler, A. Rudenko, K. Zrost, C. D. Schröter, R. Moshammer, J. Ullrich, T. Niederhausen, and U. Thumm, Complete Characterization of Molecular Dynamics in Ultrashort Laser Fields, Phys. Rev. Lett. **99**, 153002 (2007).

[23] L. Fang and G. N. Gibson, Strong-Field Induced Vibrational Coherence in the Ground Electronic State of Hot I_2, Phys. Rev. Lett. **100**, 103003 (2008).

[24] B. Fischer, M. Kremer, T. Pfeifer, B. Feuerstein, V. Sharma, U. Thumm, C. D. Schröter, R. Moshammer, and J. Ullrich, Steering the Electron in H_2^+ by Nuclear Wave Packet Dynamics, Phys. Rev. Lett. **105**, 223001 (2010).

[25] S. Erattupuzha, S. Larimian, A. Baltuška, X. Xie, and M. Kitzler, Two-pulse control over double ionization pathways in CO_2, J. Chem. Phys. **144**, 024306 (2016).

[26] A. Rudenko, V. Makhija, A. Vajdi, Th. Ergler, M. Schuerholz, R. K. Kushawaha, J. Ullrich, R. Moshammer, and V. Kumarappan, Strong-field-induced wave packet dynamics in carbon dioxide molecule, Faraday Discuss. **194**, 463 (2016).

[27] P. Agostini and L. F. DiMauro, The physics of attosecond light pulses, Rep. Prog. Phys. **67**, 813 (2004).

[28] F. Krausz and M. Ivanov, Attosecond physics, Rev. Mod. Phys. **81**, 163 (2009).

[29] E. A. Seddon, J. A. Clarke, D. J. Dunning, C. Masciovecchio, C. J. Milne, F. Parmigiani, D. Rugg, J. C. H. Spence, N. R. Thompson, K. Ueda, S. M. Vinko, J. S. Wark, and W. Wurth, Short-wavelength free-electron laser sources and science: A review, Rep. Prog. Phys. **80**, 115901 (2017).

[30] N. Gerasimova, S. Dziarzhytski, and J. Feldhaus, The monochromator beamline at FLASH: Performance, capabilities and upgrade plans, J. Mod. Opt. **58**, 1480 (2011).

[31] E. Allaria, R. Appio, L. Badano, W. A. Barletta, S. Bassanese, S. G. Biedron, A. Borga, E. Busetto, D. Castronovo, P. Cinquegrana, S. Cleva, D. Cocco, M. Cornacchia, P. Craievich, I. Cudin, G. D'Auria, M. Dal Forno, M. B. Danailov, R. De Monte, G. De Ninno *et al.*, Highly coherent and stable pulses from the FERMI seeded free-electron laser in the extreme ultraviolet, Nat. Photon. **6**, 699 (2012).

[32] F. Frassetto, N. Fabris, P. Miotti, and L. Poletto, Design study of time-preserving grating monochromators for ultrashort pulses in the extreme-ultraviolet and soft x-rays, Photonics **4**, 14 (2017).

[33] L. Poletto, P. Villoresi, F. Frassetto, F. Calegari, F. Ferrari, M. Lucchini, G. Sansone, and M. Nisoli, Time-delay compensated monochromator for the spectral selection of extreme-ultraviolet high-order laser harmonics, Rev. Sci. Instrum. **80**, 123109 (2009).

[34] M. Eckstein, C.-H. Yang, M. Kubin, F. Frassetto, L. Poletto, H.-H. Ritze, M. J. J. Vrakking, and O. Kornilov, Dynamics of N_2 dissociation upon inner-valence ionization by wavelength-selected XUV pulses, J. Phys. Chem. Lett. **6**, 419 (2015).

[35] A. von Conta, M. Huppert, and H. J. Wörner, A table-top monochromator for tunable femtosecond XUV pulses generated in a semi-infinite gas cell: Experiment and simulations, Rev. Sci. Instrum. **87**, 073102 (2016).

[36] W. Cao, G. Laurent, I. Ben-Itzhak, and C. L. Cocke, Identification of a Previously Unobserved Dissociative Ionization Pathway in Time-Resolved Photospectroscopy of the Deuterium Molecule, Phys. Rev. Lett. **114**, 113001 (2015).

[37] L. Bytautas, N. Matsunaga, and K. Ruedenberg, Accurate ab initio potential energy curve of O_2. II. Core-valence correlations, relativistic contributions, and vibration-rotation spectrum, J. Chem. Phys. **132**, 074307 (2010).

[38] C. M. Marian, R. Marian, S. D. Peyerimhoff, B. A. Hess, R. J. Buenker, and G. Seger, Ab initio CI calculation of O_2^+ predissociation phenomena induced by a spin-orbit coupling mechanism, Mol. Phys. **46**, 779 (1982).

[39] An alternative common way to illustrate resonant single- or few-photon transitions between different potential curves in intense laser field is to describe the system by a set of laser-dressed potential curves within the Floquet picture (see, e.g., S.-I. Chu and D. A. Telnov, Beyond the Floquet theorem: Generalized Floquet formalisms and quasienergy methods for atomic and molecular multiphoton processes in intense laser fields, Phys. Rep. **390**, 1 (2004) and Refs. [7,8]). A selection of the laser-dressed potential curves for relevant O_2^+ states can be found in Refs. [17–19].

[40] P. Cörlin, A. Fischer, M. Schönwald, A. Sperl, T. Mizuno, U. Thumm, T. Pfeifer, and R. Moshammer, Probing calculated O_2^+ potential-energy curves with an XUV-IR pump-probe experiment, Phys. Rev. A **91**, 043415 (2015).

[41] T. D. G. Walsh, F. A. Ilkov, and S. L. Chin, The dynamical behaviour of H_2 and D_2 in a strong, femtosecond, titanium:sapphire laser field, J. Phys. B **30**, 2167 (1997).

[42] M. R. Thompson, M. K. Thomas, P. F. Taday, J. H. Posthumus, A. J. Langley, L. J. Frasinski, and K. Codling, One and two-colour studies of the dissociative ionization and Coulomb explosion of H_2 with intense Ti:sapphire laser pulses, J. Phys. B: At., Mol. Opt. Phys. **30**, 5755 (1997).

[43] K. Sändig, H. Figger, and T. W. Hänsch, Dissociation Dynamics of H_2^+ in Intense Laser Fields: Investigation of Photofragments from Single Vibrational Levels, Phys. Rev. Lett. **85**, 4876 (2000).

[44] I. D. Williams, P. McKenna, B. Srigengan, I. M. G. Johnston, W. A. Bryan, J. H. Sanderson, A. El-Zein, T. R. J. Goodworth, W. R. Newell, P. F. Taday, and A. J. Langley, Fast-beam study of H_2^+ ions in an intense femtosecond laser field, J. Phys. B **33**, 2743 (2000).

[45] I. Ben-Itzhak, P. Q. Wang, J. F. Xia, A. M. Sayler, M. A. Smith, K. D. Carnes, and B. D. Esry, Dissociation and Ionization of H_2^+ by Ultrashort Intense Laser Pulses Probed by Coincidence 3D Momentum Imaging, Phys. Rev. Lett. **95**, 073002 (2005).

[46] A. Rudenko, B. Feuerstein, K. Zrost, V. L. B. de Jesus, Th. Ergler, C. Dimopoulou, C. D. Schröter, R. Moshammer, and J. Ullrich, Fragmentation dynamics of molecular hydrogen in strong ultrashort laser pulses, J. Phys. B **38**, 487 (2005).

[47] W. Cao, Pump-probe study of atoms and small molecules with laser driven high order harmonics, Ph.D. thesis, Kansas State University, 2014.

[48] Y. Song, M. Evans, C. Y. Ng, C.-W. Hsu, and G. K. Jarvis, Rotationally resolved pulsed field ionization photoelectron bands of $O_2^+(X^2\Pi_{1/2,3/2_g}, v^+ = 0 - 38)$ in the energy range of 12.05-18.15 eV, J. Chem. Phys. **111**, 1905 (1999).

[49] K. Ellis, R. I. Hall, L. Avaldi, G. Dawber, A. McConkey, L. Andrib, and G. C. King, High resolution threshold photoelectron and photoion spectroscopy of oxygen in the 12–50 eV photon range, J. Phys. B **27**, 3415 (1994).

[50] R. W. Nicholls, Franck-Condon factors for ionizing transitions of O_2, CO, NO and H_2 and for the $NO^+(A^1\text{-}\Sigma X^1\Sigma)$ band system, J. Phys. B **1**, 1192 (1968).

[51] O. Edqvist, E. Lindholm, L. E. Selin, and L. Åsbrink, On the photoelectron spectrum of O_2, Phys. Scr. **1**, 25 (1970).

[52] D. A. Shaw, D. M. P. Holland, E. E. Rennie, and L. G. Shpinkova, A fluorescence polarization study of the $O_2^+ A^2\Pi_u \rightarrow X^2\Pi_g$ and the $b^4\Sigma_g{}^- \rightarrow a^4\Pi_u$ transitions in the excitation range 17–25 eV, J. Phys. B **38**, 173 (2005).

[53] P. Lin and R. R. Lucchese, Theoretical studies of cross sections and photoelectron angular distributions in the valence photoionization of molecular oxygen, J. Chem. Phys. **116**, 8863 (2002).

[54] M. Magrakvelidze, C. M. Aikens, and U. Thumm, Dissociation dynamics of diatomic molecules in intense laser fields: A scheme for the selection of relevant adiabatic potential curves, Phys. Rev. A **86**, 023402 (2012).

[55] M. Magrakvelidze, A. Kramer, K. Bartschat, and U. Thumm, Complementary imaging of the nuclear dynamics in laser-excited diatomic molecular ions in the time and frequency domains, J. Phys. B **47**, 124003 (2014).

[56] S. Xue, H. Du, B. Hu, C. D. Lin, and A.-T. Le, Following coherent multichannel nuclear wave packets in pump-probe studies of O_2 with ultrashort laser pulses, Phys. Rev. A **97**, 043409 (2018).

[57] P. H. Bucksbaum, A. Zavriyev, H. G. Muller, and D. W. Schumacher, Softening of the H_2^+ Molecular Bond in Intense Laser Fields, Phys. Rev. Lett. **64**, 1883 (1990).

[58] J. McKenna, A. M. Sayler, F. Anis, B. Gaire, N. G. Johnson, E. Parke, J. J. Hua, H. Mashiko, C. M. Nakamura, E. Moon, Z. Chang, K. D. Carnes, B. D. Esry, and I. Ben-Itzhak, Enhancing High-Order Above-Threshold Dissociation of H_2^+ Beams with Few-Cycle Laser Pulses, Phys. Rev. Lett. **100**, 133001 (2008).

[59] J. McKenna, F. Anis, A. M. Sayler, B. Gaire, N. G. Johnson, E. Parke, K. D. Carnes, B. D. Esry, and I. Ben-Itzhak, Controlling strong-field fragmentation of H_2^+ by temporal effects with few-cycle laser pulses, Phys. Rev. A **85**, 023405 (2012).

[60] B. Feuerstein and U. Thumm, Mapping of coherent and decohering nuclear wave-packet dynamics in D_2^+ with ultrashort laser pulses, Phys. Rev. A **67**, 063408 (2003).

[61] X. M. Tong and C. D. Lin, Attosecond xuv pulses for complete mapping of the time-dependent wave packets of D_2^+, Phys. Rev. A **73**, 042716 (2006).

[62] L. Fang and G. N. Gibson, Investigating excited electronic states of I_2^+ and I_2^{2+} produced by strong-field ionization using vibrational wave packets, Phys. Rev. A **75**, 063410 (2007).

[63] V. L. B. de Jesus, A. Rudenko, B. Feuerstein, K. Zrost, C. D. Schröter, R. Moshammer, and J. Ullrich, Reaction microscopes applied to study atomic and molecular fragmentation in intense laser fields: Non-sequential double ionization of helium, J. Electron Spectrosc. Relat. Phenom. **141**, 127 (2004).